

Volume 2, Number 2, pp. 118-129, 2000.



# Spiral Wave Dynamics in Two Dimensional Isotropic Models of Mammalian Ventricular Tissue

G. P. Kremmydas\* and A. V. Holden\*\*

\* Ionian Centre for Science & Technology, Argostoli GR281 00, Kefalonia, Greece \*\* School of Biomedical Sciences, University of Leeds, Leeds, LS2 9JT, United Kingdom

Correspondence: george@cbiol.leeds.ac.uk

Abstract. We characterise the effects of ionic conductance and concentration changes on the meandering patterns and dynamics of re-entrant excitation in a model of mammalian ventricular tissue. A two-dimensional reaction-diffusion system with kinetics described by the Oxsoft <sup>®</sup>Heart equations for the single guinea pig ventricular cell was used. The development and stability of re-entrant spiral wave solutions is examined. The effects of ionic conductance and concentration changes on spiral-wave meandering are investigated. Spiral wave meandering behaviour provides a significant validation test for detailed biophysical models and can prove a valuable tool for theoretical investigations in cardiac pathophysiology.

Keywords: reentry, spiral-wave, excitable medium, meandering

### Introduction

Reentrant cardiac arrhythmias are characterised by the repeated reinvasion of the same region of the tissue by the same wave front propagation around an anatomical obstacle. Simple reentry may produce monomorphic ventricular tachycardia patterns while ventricular fibrillation may also be due to reentrant waves. Reentry can be idealised as spiral wave solutions in homogenous excitable media. In this paper we characterise the dynamics of spiral wave reentry by analysing the development, stability and meandering of spiral waves in a two dimensional model of ventricular tissue and their dependence on ionic conductance and ionic concentration changes. Developments in experimental cardiac electrophysiology have provided a vast amount of information on the mechanisms underlying excitation and propagation in cardiac tissue. The results of voltage clamp experiments on ventricular cells and tissue have been incorporated in a number of mathematical models for ventricular excitation [1,12,13,14,15]. None of the available models can be regarded as complete as the ongoing process of modelling the behaviour of different types of ventricular cells with biophysicaldetailed models is constantly pushed forward as new experimental data accumulate. In this paper we use the ordinary differential equations of the Oxsoft ®Heart guinea-pig ventricle (GPV) model to construct an excitable medium for mammalian ventricular tissue by incorporating them into a reaction diffusion system of equations [5].

## **Methods**

In the simulations that follow the  $Oxsoft^{\circledR}$  Heart guinea-pig ventricle model (described in detail in [5]) was used. The partial differential equations for ventricular action potential propagation were numerically integrated as in [6] using a space step of 100  $\mu$ m and a time step of 50  $\mu$ s. The diffusion coefficient was set to 31.25 mm<sup>2</sup>s<sup>-1</sup> to give a plane-wave propagation speed of 0.6 ms<sup>-1</sup>. Unless otherwise stated the numerical integration was on a medium of 20 mm  $\times$  20 mm. Spiral wave re-entry was initiated in a homogenous and isotropic two dimensional medium using the phase distribution method [6]. The spiral-wave tip was identified as the intersection of the isolines of membrane potential V = -10 mV and of Ca<sup>2+</sup> gating variable f = 0.5. Spiral wave meandering patterns were recorded in simulations of 3s duration. The initial transient trajectory of the spiral tip [6] was ignored and meandering was compared for a given duration. Simulations were repeated for different ionic conductance and ionic concentration parameters for each of the main ionic species Na<sup>2+</sup>, K<sup>+</sup> Ca<sup>2+</sup>. Tip trajectories obtained for simulations with different values of the same parameter were compared during the same time interval and after removing transient trajectory segments of the same duration.

## **Results**

### Standard meandering.

Spiral waves in the standard guinea-pig ventricular tissue model meander around an inexcited core. The core region is rendered inexcitable by the local inactivation of  $I_{\text{Na}}$  current. Figure 1 shows a spiral wave solution and the evolution of the spiral tip trajectory for the standard GPV model. Standard parameter values given in [5] where used. After following an initial large transient trajectory the spiral-tip rotates around a core restricted in a region with a size of a few mm. The 5-lobe pattern of the tip meandering evolves and changes with time. This trajectory "aging" process has been described in [5] and is attributed to the slow changes in intracellular concentrations that take place in  $Oxsoft^{(8)}$  Heart models for simulations of long duration. The reduction of the wavefront velocity near the functional block developed around the spiral core is due to the propagation of the wave-front into the region of refractory tissue [6]. The wavefront driven by  $I_{\text{Na}}$  can not propagate deep into the core region where it is inactivated but  $I_{\text{Ca}}$  can carry the wave-front into the refractory region.

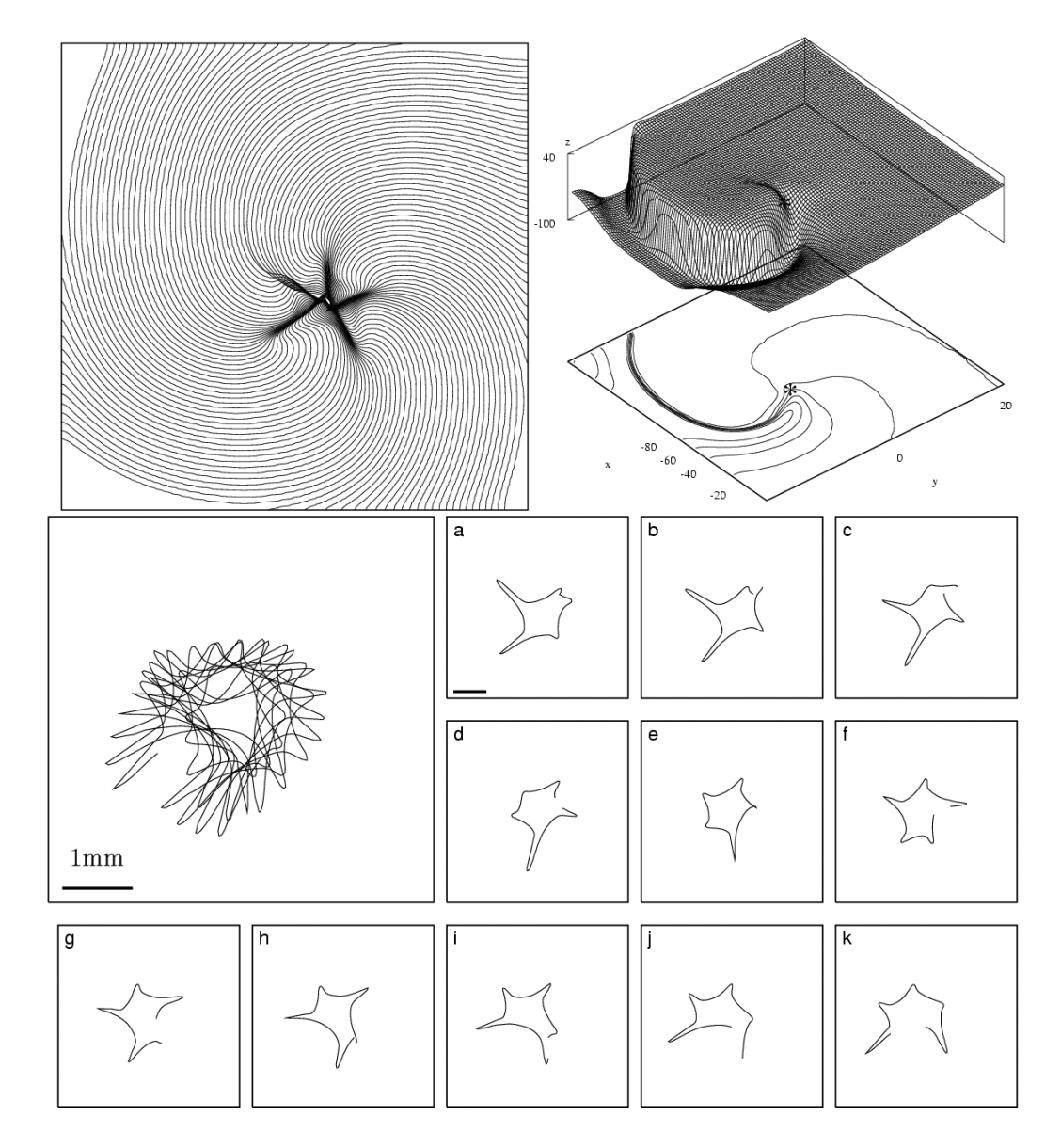


Figure 1. Spiral-wave solution and tip-trajectory evolution for the "normal" guinea-pig ventricular model. (a) Isochrones of the wavefront shown every 1ms. A total of 105 isochrones are plotted (average rotation period is approximately 100ms throughout the simulation). (b) Spatial voltage distribution (V -> z-axis) snapshot. The numbers at the bottom of the plot indicate the V-level contours and the asterisk the position of the spiral tip. (c) Tip trajectory evolution for the "normal" guinea-pig ventricular model (standard parameter values used see [5]). The region shown here is  $5.5 \times 5.5$  mm<sup>2</sup>. The enlarged panel shows tip trajectory evolution for 1100ms starting at t = 1900ms to remove transients. Panels a-k show the same evolution in segments of 100ms. The horizontal solid bar in the enlarged and the first panel is 1mm wide. Mp4 movie of spiral-wave reentry in the guinea-pig ventricle model (white: excitation wave-front).

#### Spiral-wave breakup.

The spiral wave solution of Figure 1 is sensitive to the dynamics of the calcium current. Figure 2 shows 10 ms snapshots of the spatial distribution of membrane potential V(x, y) starting at t = 0 ms where in each frame the black region corresponds to points with V(x, y) = -10 mV. In the first three rows (first 260 ms of the simulation) variations in the the impulse width throughout the wavefront are observed. In the fourth row the impulse width seems to get reduced due to a local conduction block which leads to excitation-wave breakup. Successive evolution gives rise to complex excitation patterns. Organising centres are created through breakup but also extinguished through collision and annihilation. Under

such conditions the degeneration of excitation patterns into turbulent activity depends on the net rate of "birth" of spiral-wave organising centres through breakup (i.e. rate of breakup minus rate of annihilation of organising centres) and the size of the medium.

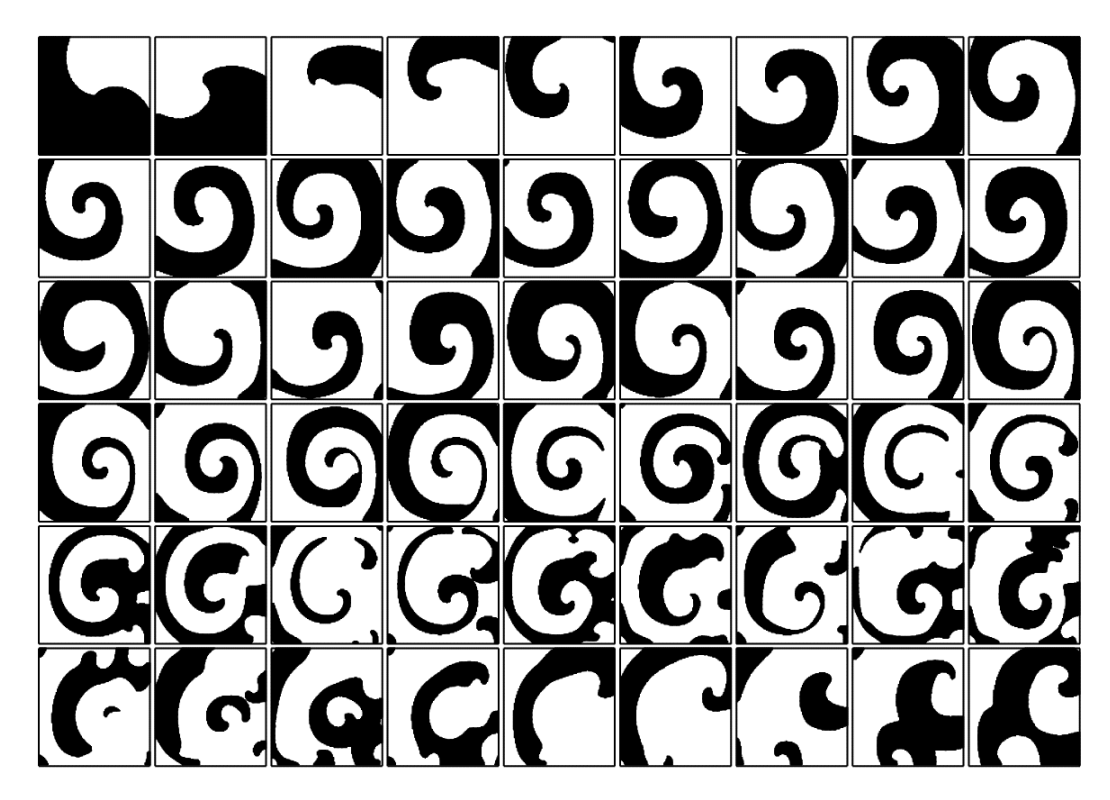


Figure 2. Spiral wave break-up in the guinea-pig ventricular model. For this simulation  $P_{Ca}$  was set to zero. The region with V >= -10 mV is plot (black area) in consecutive snapshots every 10 ms (left to right starting from the top). Medium size is  $20mm \times 20$  mm. Mp4 movie of spiral-wave breakup in the guinea-pig ventricle model (black: excited, white: excitable).

#### Sprouting.

Broken wave-fronts can give rise to spiral waves if the excitability of the medium is high enough. Figure 3 shows the sprouting of a broken excitation wavefront in the normal GPV medium. A plane wave is initiated by a supra-threshold stimulus at the lower bottom of the medium. Before the wavefront reaches the middle of the route to the top boundary the left 3/4 of the medium are set to resting state. The broken wavefront tip thus produced sprouts to the left and bottom of the medium while the rest part of the wavefront continues its propagation towards the top. The solid line in the plots of Figure 3 denotes the V = -10 mV isoline while dashed one indicates the tip trajectory (i.e. the intersection of V = -10 mV and f = 0.5 isolines). The wave-tip rapidly returns towards the refractory tail of the propagating wave. Thus, theinitial tip-trajectory is almost linear with a direction towards the bottom of the medium. The speed and direction of tip movement should not be confused with the local propagation velocity and the evolution of the wave-front line at different segments across its whole length that depend on the local curvature. The latter varies and is different from the curvature at the wavefront tip (critical curvature). After this phase, the sprouting tip bypasses the refractory tail of the wavefront and returns to excite the recovered region behind it. The plots in Figure 3 are shown every 5ms while the total simulation time is 55ms.

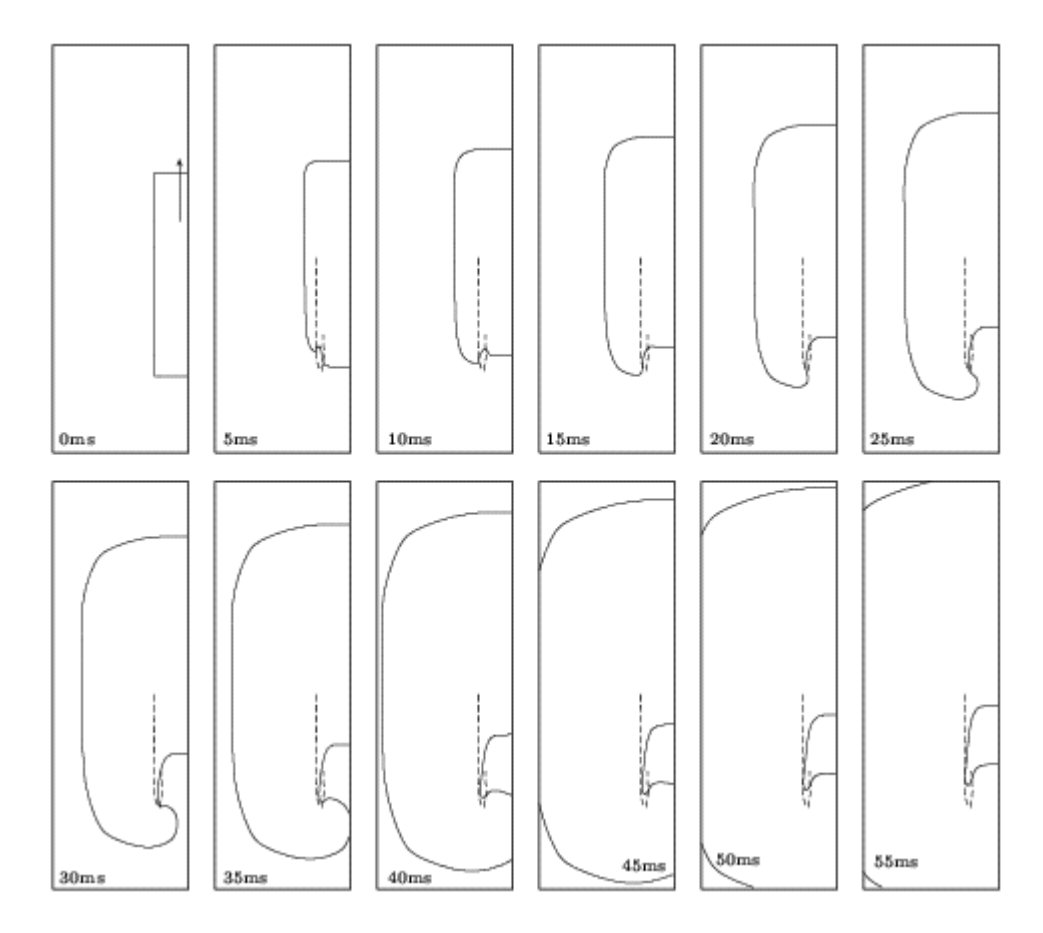


Figure 3. Sprouting of a broken excitation wavefront for the standard guinea-pig ventricular model. The solid line corresponds to the V = -10 mV isoline and the dashed one to the tip trajectory (intersection of V = -10 mV and f = 0.5 isolines). In the first plot the cut excitation-wave is shown. This was obtained by stimulating at the bottom of the medium and after the wavefront propagated for awhile setting 3/4 of the left side of the medium to the resting state. Snapshots are shown every 5ms (left to right starting from top left). The medium size is 20mm  $\times$  60mm.

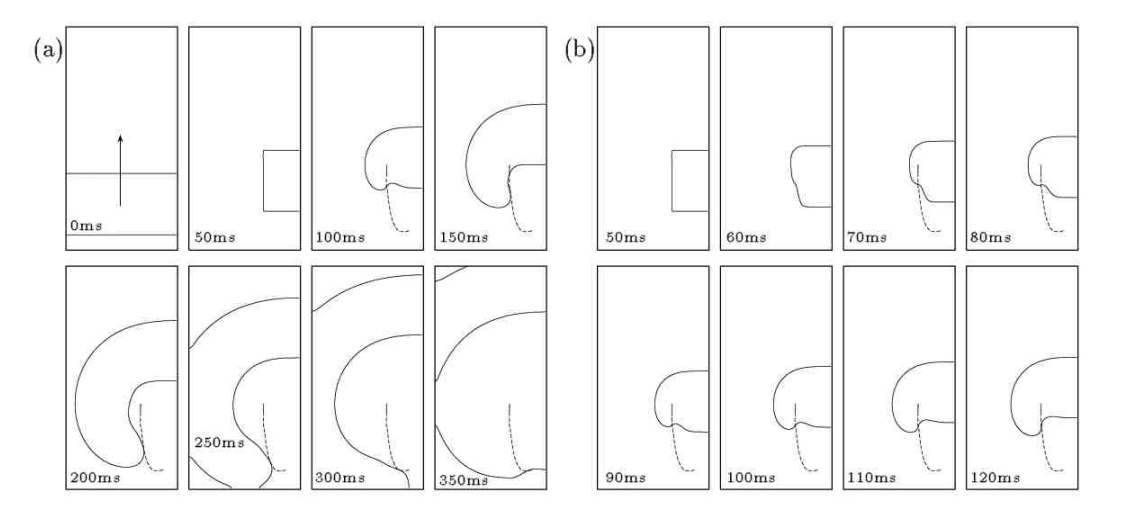


Figure 4. Sprouting of a broken excitation wavefront for the guinea-pig ventricular model with low excitability ( $g_{Na}=0.3$  mS). The solid line corresponds to the V=-10 mV isoline and the dashed one to the tip trajectory (intersection of V=-10 mV and f=0.5 isolines). In the second frame of plot (a) the cut excitation-wave is shown. This was obtained by stimulating at the bottom of the medium and after the wavefront propagated for awhile setting 2/3 of the left side of the medium to the resting state. Snapshots in (a) are shown every 50 ms (left to right starting from top left). In plot (b) the same

simulation is shown starting from the time the wavefront was cut with successive frames shown every 10ms. The medium size is  $20 \text{ mm} \times 40 \text{ mm}$ .

This sprouting scenario is altered if the medium excitability is appropriately modified. In Figure 4 the same computational experiment is repeated for a guinea-pig ventricle model for which the medium excitability is significantly reduced by setting the sodium conductance g<sub>Na</sub>to 0.3mS the standard value being 2.5 mS (medium size: 20 mm×40 mm). Figure 4.a the broken wave produced by setting 2/3 of the left side of the medium to the resting stateafter a propagating planar wave has been initiated. The V = -10 mV isoline (solid line) is plotted every 50 ms with the dashed line representing the wave-tip evolution during the simulation. Due to the low excitability local propagation of the wavefront - including the wave-tip - is slower. The wave-tip trajectory is curved while the speed of its movement is a lot slower than the propagation of the wavefront. The refractory wave tail is not closely followed by the wave-tip in this case. In Figure 4.b the initial evolution of the broken excitation-wave is shown at smaller time intervals (plots every 10 ms). This plot shows how the refractory part of the broken-end of the wave slowly retracts while the excitatory part sprouts. The excitatory and refractory portions of the broken end are separated by the point of intersection of the wave-tip trajectory (dashed line) and the V-isoline. This was obtained by stimulating at the bottom of the medium and after the wavefront propagated for awhile setting 2/4 of the left side of the medium to the resting state. Snapshots in (a) are shown every 50 ms (left to right starting from top left). In plot (b) the same simulation is shown starting from the time the wavefront was cut with successive frames shown every 10 ms.

### Meandering

The dependence of spiral-wave tip meandering patterns on the conductance of the principal ionic currents and ion concentrations is illustrated in the following simulations.

### Transient outward conductance $g_{to}$

The transient outward current,  $I_{to}$  has been reported to occur in different cell types and it is mainly carried by  $K^+$  ions. Its activation, inactivation and reactivation are voltage dependent. In canine ventricular tissue  $I_{to}$  is prominent in the epicardium but not in the endocardium. In the guinea-pig ventricular cell model we manipulate  $I_{to}$  by modifying  $g_{to}$  i.e. the maximum transient outward channel conductance. The behaviour of the model for the standard  $g_{to}$  value (0.005 mS), double and half the standard value and also  $g_{to} = 0$  is shown in Figure 5. The timeseries of V shown in Figure 5(b) and (c) are obtained as "point-electrode" recordings from an one-dimensional simulation during which the cable is stimulated at one end. In (b) a single stimulus and in (c) repetitive stimuli were applied. The meandering patterns shown in Figure 5(a) show no significant differences between the normal meandering pattern (5.a.I) and that obtained for the reduced (5.a.III) or blocked  $g_{to}$  meandering pattern. When  $g_{to}$  is increased from the standard value (5.a.IV) the central core relatively reduced in size but a larger 5-lobe meandering pattern is observed.

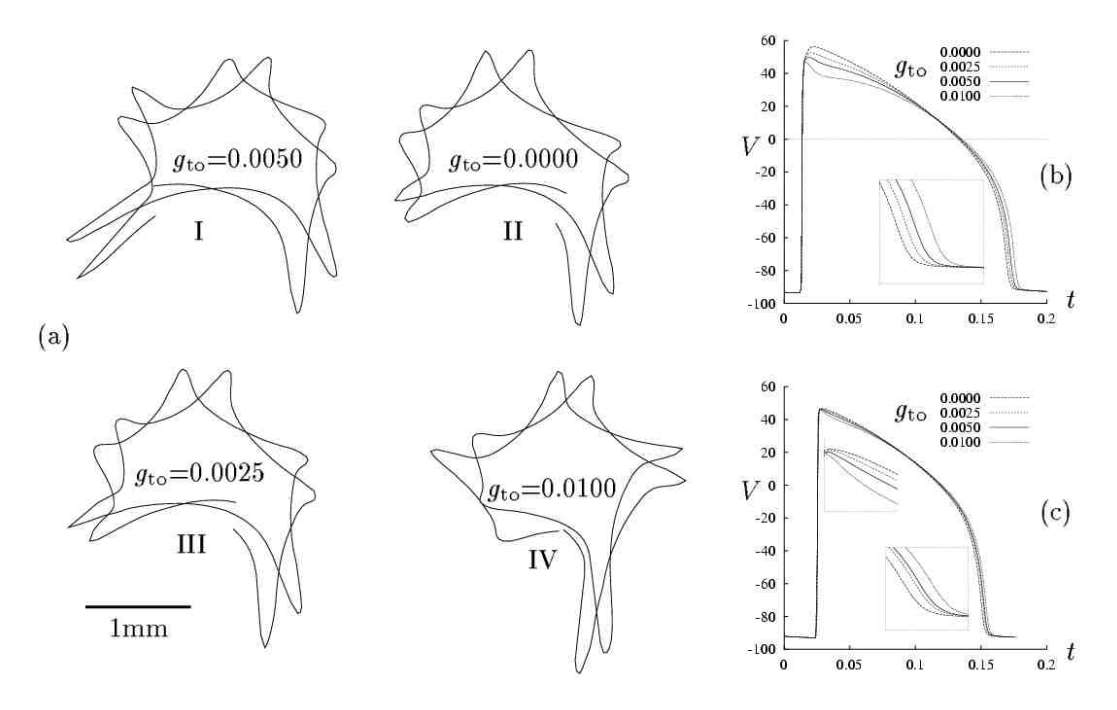


Figure 5. Effects of  $g_{to}$  on spiral-wave meandering patterns. (a) Tip-trajectory evolution for different  $g_{to}$  values during 220 ms. (a.I) $g_{to} = 0.0050$  mS is the value for the standard guinea-pig ventricle model, (a.II)  $g_{to} = 0.0$  mS - $I_{to}$  is blocked, (a.III)  $g_{to} = 0.0025$  mS -half the standard value, (a.IV)  $g_{to} = 0.01$  mS - double the standard value. Action potential configurations with different  $g_{to}$  values are shown superimposed for single (b) and repetitive stimulation (c). The inset plots in (b) and (c) are magnifications of the corresponding parts of the main plot. The  $g_{to}$  values are given in the legend (t in s, Vin mV).

#### Sodium conductance $g_{Na}$ .

The sodium current is the dominant current during the rising phase of the action potential and its amplitude affects the depolarisation rate (quantified by the maximum  $\mathrm{d}V/\mathrm{d}t$ ) and thus the conduction velocity of activation wavefronts in cardiac tissue. The persistent inactivation of  $I_{\mathrm{Na}}$  is responsible for the inexcitable spiral core around which spiral wave rotation is organised in two dimensions. Moreover, it has been suggested [6] that the interaction of  $I_{\mathrm{Na}}$  and  $I_{\mathrm{Ca}}$  wave fronts underlies the meandering patterns in models of mammalian ventricular tissue.

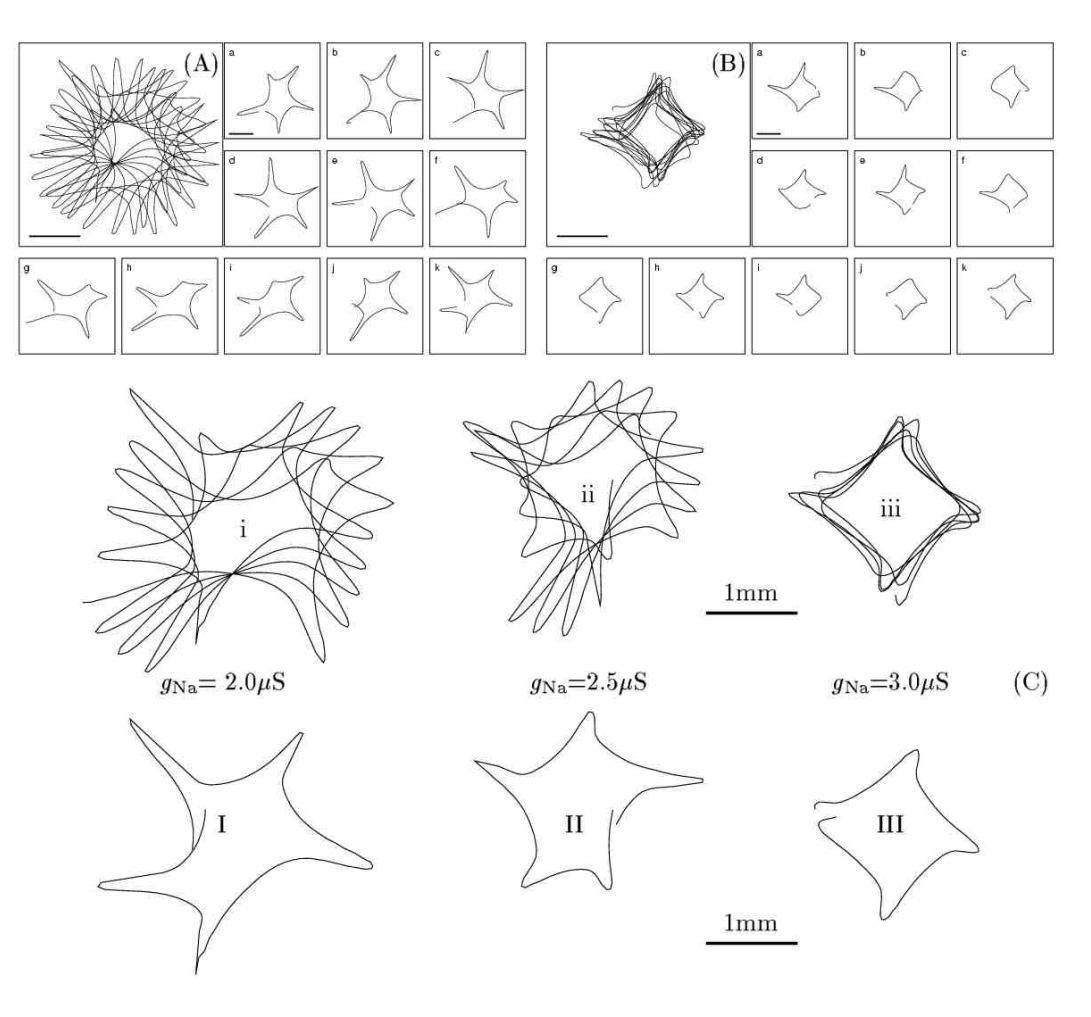


Figure 6. Effect of  $g_{Na}$  on meandering patterns. (C) Tip-trajectory evolution during 500 ms (i-iii) and 110 ms (I-III). for different  $g_{Na}$  values: (C.i,I) $g_{Na} = 2.0$  mS, (C.ii,II)  $g_{Na} = 2.5$ mS - standard value for guinea-pig ventricular model, (C.iii,III) $g_{Na} = 3.0$ mS. The evolution of the spiral tip-trajectory is shown in (A) for  $g_{Na} = 2.0$  mS and (B) for  $g_{Na} = 3.0$  mS. In the enlarged panel of (A) and (B) the total duration of tip-trajectory evolution is 1100 ms corresponding to the interval 1400-2500 ms of simulation in which a spiral was initiated using the phase distribution method. The corresponding plots (a-k) show thesame simulation in successive 100 ms intervals. The region shown here is  $4.0 \times 4.0$  mm<sup>2</sup>. The horizontal solid bars are 1 mm long.

Pathophysiological or pharmaceutical interventions that alter the sodium conductance  $g_{\text{Na}}$ would significantly affect the dynamics of spiral wave reentry in cardiac muscle. Such effects are demonstrated in Figure 6 for the guinea-pig ventricular model. Meandering patters of spiral wave tip for the standard configuration are compared with the ones obtained with increased and decreased  $g_{\text{Na}}$ . The reduction of  $g_{\text{Na}}$  (Figures 6 A, I and i) expands the region of sodium current inactivation as the  $I_{Na}$  waves die earlier due to their decreased amplitude. In addition to the increase of the meandering core the lobes of the pattern are longer. This suggests that the region of functional block is invaded deeper, possibly due to the slower  $I_{\text{Ca}}$ wave [6]. On the other hand, increasing  $g_{Na}$  (Figures 6 B, III and iii) reduces the core size and suppresses the 5-lobe pattern. An almost square core with four small lobes emerges. In Figure 6.B the aging process of the spiral core for increased  $g_{Na}$  is shown. It can be seen that the initially more pronounced 4-lobe meandering pattern gets suppressed into an almost square trajectory. The increase of  $g_{Na}$  strengthens the  $I_{Na}$  wave and alters the dynamical interaction of  $I_{Na}$  and  $I_{Ca}$  waves close to the spiral core. This results in decreasing the persistent  $I_{Na}$  inactivation region so that the slow  $I_{Ca}$  wave is not strong enough to bring the excitation wavefront deeper in the refractory region.

## Potassium conductance $g_{K1}$ .

The potassium current  $I_{K1}$  is activated during the falling phase of the action potential and contributes to the repolarisation of cardiac tissue. Its modification would affect the action potential duration by altering the repolarisation rate mainly during the late repolarisation phase. Figures 7.b and 7.c illustrate the effect of altering  $g_{K1}$  on the action potential for single and repetitive stimulation respectively. Reducing  $g_{K1}$  prolongs while increasing  $g_{K1}$ shortens action potential duration although  $g_{K1}$  are less pronounced under repetitive stimulation. Meandering patterns obtained by manipulating  $g_{K1}$  are shown in Figure 7.a. For low  $g_{K1}$  the normal 5-lobe meandering pattern is altered with the lobe size being diminished around a central core of size comparable to the standard one. This lobe-suppression effect is similar to but not the same as in the case of increased  $g_{Na}$  (Figure 6). The increase of  $g_{K1}$  increases the meandering region by extending the lobe length of the tip-trajectory pattern.

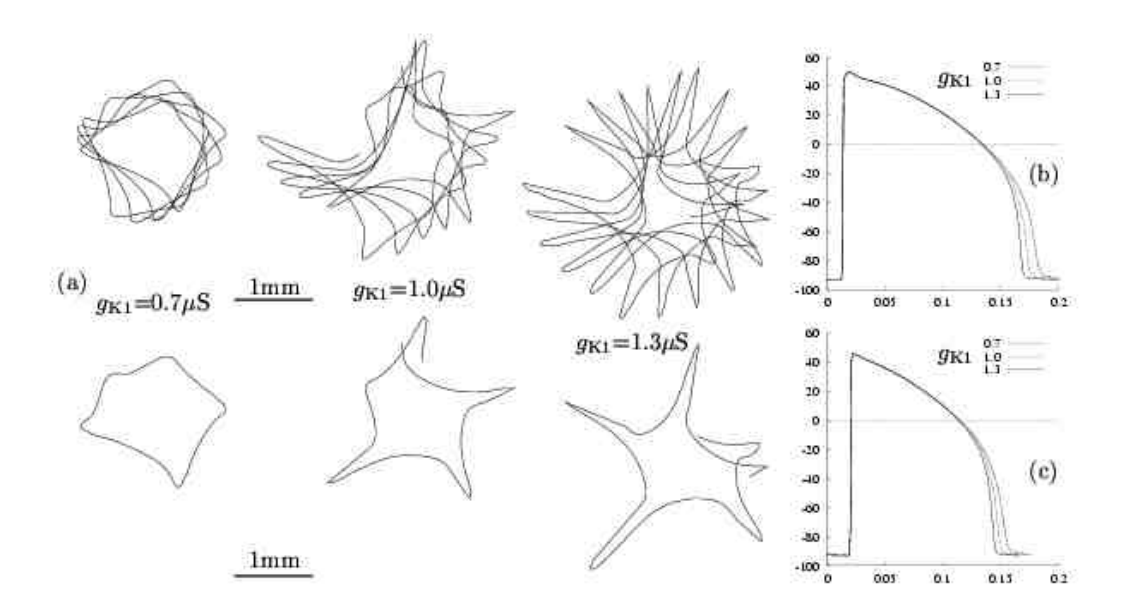


Figure 7. Effects of  $g_{K1}$  on spiral-wave meandering patterns. (a) Tip-trajectory evolution for different  $g_{K1}$  values during 500 ms (top) and 110 ms (bottom). The middle trajectory corresponds to  $g_{K1} = 1.0$  mS which is the value for the standard guinea-pig ventricle model. Action potential configurations with different  $g_{K1}$  values are shown superimposed for single (b) and repetitive stimulation (c). The  $g_{K1}$  values (in mS) are given in the legend (t in s,V in mV).

#### Calcium conductance.

In the guinea-pig ventricular model the magnitude of  $I_{\text{Ca}}$  can be modulated via  $P_{\text{Ca}}$ , the permeability of the slow inward calcium channel. Figure 8.c shows the restitution curves for different values of  $P_{\text{Ca}}$ . Action potential duration is normally increased with the increase of  $P_{\text{Ca}}$ .

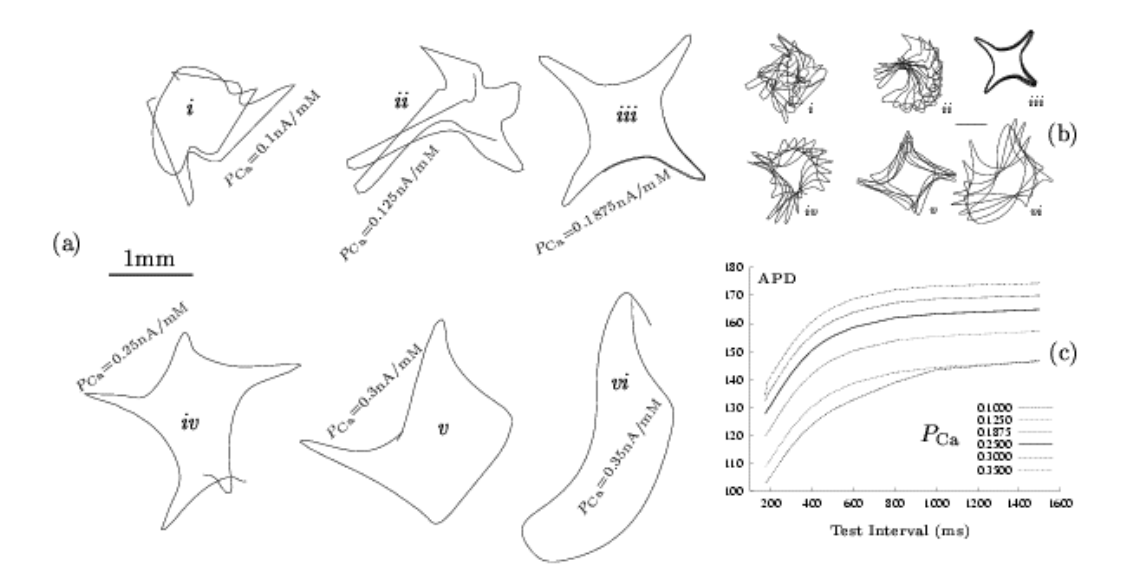


Figure 8. Effects of altering  $P_{Ca}$  on spiral-wave meandering. The evolution of the tiptrajectory is shown for 120 ms (a) and 600 ms (b). For the standard configuration (a.iv), (b.iv)  $P_{Ca} = 0.25$  nA/mM while for the other plots: (a.i),(b.i)  $P_{Ca} = 0.1$  nA/mM, (a.ii), (b.ii)  $P_{Ca} = 0.125$  nA/mM, (a.iii),(b.iii)  $P_{Ca} = 0.1875$  nA/mM, (a.v),(b.v)  $P_{Ca} = 0.3$  nA/mM, (a.vi),(b.vi)  $P_{Ca} = 0.35$  nA/mM. In plot (c) the corresponding restitution curves are shown. The horizontal solid bar in (a) and (b) is 1mm long. The simulations were run in a 20 mm  $\times$  20 mm homogenous medium in which a counter-clockwise rotating spiral was initiated.

Meandering patterns for different values of  $P_{\text{Ca}}$  are shown in Figure 8.a,b. The standard value for P<sub>Ca</sub> is 0.25 nA/mM for which the 5-lobe meandering pattern is observed. With PCareduced to 0.1875 nA/mM (fig. 8.a.iii) a 4-lobe meandering pattern with pronounced lobe length is obtained. This 4-lobe pattern has a striking property that can be visualised from Figure 8.b.iii: it is a lot more stable than other meandering patterns as its shape is not significantly changed or displaced with time. At lower values more complex patterns are obtained with the core size being reduced in general. As  $P_{\text{Ca}}$  tends to zero irregularities in spiral wave activity are observed as the spiral waveform changes with time and space. For values very close to zero as one moves from the tip along the excitation wavefront the distance between the excitation wavefront and the refractory tail varies with distance as well as time. Such instabilities have been described for other models [8] and seem to lead to spiral wave break up. Indeed for the guinea-pig ventricular model  $P_{\text{Ca}}$  seems to be a parameter that can lead to transition into irregular behaviour as illustrated in section §3.2. For increased  $P_{\text{Ca}}$ a square-like meandering pattern is also obtained (fig. 8.b.v) with a central core larger than that for reduced  $P_{\text{Ca}}$  (fig. 8.b.iii) and the four lobes of varying size with time but less pronounced than in fig. 8.b.iii. With  $P_{\text{Ca}}$  further increased (fig. 8.b.vi) the spiral core becomes more elongated and lobe patters tend to get suppressed both with time for a given  $P_{\text{Ca}}$  value or with increasing  $P_{\text{Ca}}$ .

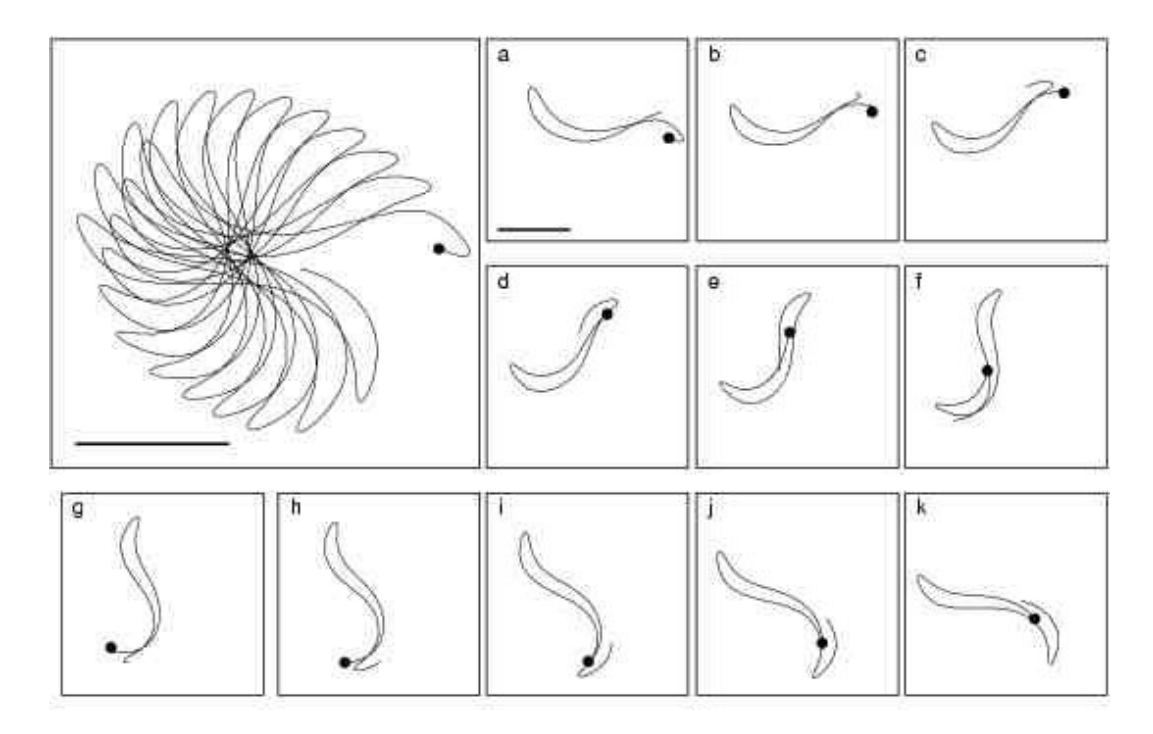


Figure 9. Meandering pattern for  $P_{Ca} = 0.5$  (standard value is  $P_{Ca} = 0.25$ ). Plots a-k show tip-trajectory evolution during successive 150 ms intervals while the enlarged plot shows the whole evolution from a to k. The starting tip-trajectory point in each plot is marked by a filled circle. The horizontal bars correspond to 5 mm and the plot size is  $14 \text{ mm} \times 14 \text{ mm}$ . The simulation consisted of a counter-clockwise rotating spiral in a  $30 \text{ mm} \times 30 \text{ mm}$  homogenous guinea-pig ventricular medium.

If  $P_{\text{Ca}}$  is doubled from its standard value an almost linear core is obtained as it can be seen from Figure 9. Plotted during one rotation the tip-trajectory is reminiscent of that obtained for the Fitz Hugh-Nagumo medium in [9].

# **Conclusions**

Calcium conductance blockade has been used in [8] and was found to remove the extended conduction blocks responsible for the onset of irregular activation patterns. On the contrary calcium conductance blockade in the guinea-pig ventricular model seems to be responsible for spiral wave break-up and the onset of irregular activation patterns (see Figure 2). Most commonly excitable media models support spiral waves that are stable in the sense that asingle spiral wave-front exists emanating from the core. This single-spiral might be rigidly rotating, meandering or drifting but its waveform is stable [2, 4, 3]. Chudin et al [7] study excitation wave propagation in cardiac tissue and the effects of intracellular calcium dynamics using the modified Luo-Rudy model [10, 11, 12, 13]. They report irregular dynamical behaviour for intracellular calcium in single-cell simulations with high frequency stimulation. It is suggested that this behaviour underlies the transition from stationary spiralwave to the spiral-wave breakup regime. In their two dimensional simulations (excitable medium model with modified Luo-Rudy kinetics implemented on aparallel supercomputer CRAY-T3D) spiral waves degenerate to fibrillation due to wave breakup. Using the singlecell results the authors propose that the transition from the stationary to the non-stationary spiral wave behaviour is due to the slow development of complex Ca<sup>2+</sup> dynamics: the elevation of the internal Ca<sup>2+</sup>concentration increases the action potential duration by amplifying the Na<sup>+</sup>-Ca<sup>2+</sup>exchanger current. This prolongation of APD shortens the diastolic interval and modifies the character of propagation with a critical point being the abnormally high Ca<sup>2+</sup> release from the sarcoplasmic reticulum [7]. This hypothesis was tested through two dimensional simulations with the L-type Ca<sup>2+</sup> channel blocked. The channel blockade produced stable spiral waves (no breakup was observed) while if applied after initial breakup process it could prevent the cascade of breakup and the degeneration of excitation patterns into turbulent activity [7]. In the *Oxsoft* <sup>®</sup>*Heart* guinea-pig ventricular model  $I_{Ca}$  we conducted two-dimensional simulations of spiral-wave activity for which the parameter  $P_{Ca}$  (calcium channel permeability) was varied over a wide range of parameter-values. Increasing or decreasing  $P_{Ca}$  is correspondingly increasing or decreasing the flow of  $Ca^{2+}$  ions into the cell without affecting the passage of  $K^+$ ,  $Na^+$  through the  $Ca^{2+}$  channel. In almost all simulations stable spiral wave activity was sustained although the modification of  $P_{Ca}$  significantly affected the spiral-wave tip meandering patterns. The spiral wave breakup behaviour observed here is similar to that obtained by Chudin *et al* [7] but the mechanism producing this behaviour in the two models seems to be quite opposite. In the simulations of Chudin *et al* [7] preventing calcium entry into the cells through L-type  $Ca^{2+}$  channel blockade inhibited breakup while in our simulations preventing calcium entry through the reduction of  $P_{Ca}$  favoured breakup.

## References

- [1] Beeler, G.W. and Reuter, H., "Reconstruction of the action potential of ventricular myocardial fibres", Journal of Physiology, vol. 268, pp. 177-210, 1977.
- [2] Biktashev, V.N. and Holden, A.V., "Resonant drift of an autowave vortex in a bounded medium", Physics Letters A, vol. 181, pp. 216-224, 1993.
- [3] Biktashev, V.N. and Holden, A.V., "Design principles of a low-voltage cardiac defibrillator based on the effect of feedback resonant drift", Journal of Theoretical Biology, vol. 169, pp. 101-112, 1994.
- [4] Biktashev, V.N. and Holden, A.V., "Resonant drift of autowave vortices in 2 dimensions and the effects of boundaries and inhomogeneities", Chaos Solitons & Fractals, vol. 5, pp. 575-622, 1995.
- [5] Biktashev, V.N. and Holden, A.V., "Re-entrant activity and its control in a model of mammalian ventricular tissue", Proceedings of the Royal Society of London Series B- Biological Sciences, vol. 263, pp. 1373-1382, 1996.
- [6] Biktashev, V.N. and Holden, A.V., "Reentrant waves and their elimination in a model of mammalian ventricular tissue", Chaos, vol. 8, pp. 48-56, 1998.
- [7] Chudin, E., Garfinkel, A., Weiss, J., Karplus, W. and Kogan, B., "Wave propagation in cardiac tissue and effects of intracellular calcium dynamics (computer simulation study)", Progress in Biophysics & Molecular Biology, vol. 69, pp. 225-236, 1998.
- [8] Courtemanche, M. and Winfree, A., "Re-entrant rotating waves in a beeler-reuter based model of two-dimensional cardiac activity", International Journal of Bifurcations & Chaos, vol. 1, pp. 431-444, 1991.
- [9] V. Krinsky, I. and Efimov, I.R., "Vortices with linear cores in mathematical-models of excitable media", Physica A, vol. 188, pp. 55-60, 1992.
- [10] Luo, C.H. and Rudy, Y., "A model of the ventricular cardiac action-potential depolarization, repolarization, and their interaction", Circulation Research, vol. 68, pp. 1501-1526, 1991.
- [11] Luo, C.H. and Rudy, Y., "A dynamic-model of the cardiac ventricular action-potential ionic currents and concentration changes", Circulation, vol. 86, pp. 563, 1992.
- [12] Luo, C.H. and Rudy, Y., "A dynamic-model of the cardiac ventricular action-potential .1. simulations of ionic currents and concentration changes", Circulation Research, vol. 74, pp. 1071-1096, 1994.
- [13] Luo, C.H. and Rudy, Y., "A dynamic-model of the cardiac ventricular action-potential .2 afterdepolarizations, triggered activity, and potentiation", Circulation Research, vol. 74, pp. 1097-1113, 1994.
- [14] Noble, D., Noble, S.J., Bett, G.C.L., Earm, Y.E., Ho, W.K. and So, I.K., "The role of sodium-calcium exchange during the cardiac action- potential", Annals of the New York Academy of Sciences, vol. 639, pp. 334-353, 1991.
- [15] Oxsoft. Oxsoft ® Heart. Program manual Version 4.4, 1994.

